Sensor and Simulation Notes

Note 523

20 August 2007

Combined Electric and Magnetic Dipoles for Mesoband Radiation

Carl E. Baum
University of New Mexico
Department of Electrical and Computer Engineering
Albuquerque New Mexico 87131

Abstract

This paper explores a new possible type of high-power mesoband radiator. This consists of a pair of dipoles, one electric and one magnetic, with aligned vectors, but $\pi/2$ (90°) out of phase. This gives a circular polarization in the far field.

`

This work was sponsored in part by the Air Force Office of Scientific Research.

1. Introduction

For mesoband high-power radiators [21] we need appropriate antennas to radiate the energy from some source such as a switched oscillator. Various types are possible [12-18, 20]. Here we consider yet another kind.

Noting that the switched oscillator can be described by a resonant circuit (for frequencies of interest), we can consider a combination of loop (magnetic dipole) and electric dipole as a resonant circuit matched to the source in an appropriate way. By making the magnetic dipole moment $\vec{m}$ parallel to the electrical dipole moment $\vec{p}$, but out of phase by $\pi/2$ (90°) we can achieve approximate circular polarization in the far field.

2. Crosspolarized Electric and Magnetic Dipoles, $\pi/2$ Out of Phase

Consider the basic antenna geometry in Fig. 2.1, which schematically illustrates the approach. Here we have electric and magnetic dipole moments given by

$$\begin{aligned} &\tilde{\vec{p}}(s) = \vec{1}_z\, \tilde{p}(s) \quad , \quad \tilde{\vec{m}}(s) = \vec{1}_z\, \tilde{m}(s) \\ &s \equiv \Omega + j\omega \equiv \text{Laplace-transform variable or complex frequency} \\ &\sim \equiv \text{Laplace transform (two-sided)} \end{aligned} \tag{2.1}$$

Our concern here is with a parallel resonant frequency

$$\begin{aligned} s_0 &= j\omega_0 \\ \omega_0 &= \left[\mathrm{L}_h \mathrm{C}_e\right]^{-1/2} \end{aligned} \tag{2.2}$$

There are also radiation losses which shift s_0 over into the left half plane [LHP]. Such are not included in the present analysis.

Here we have cylindrical (Ψ, ϕ, z) coordinates

$$\begin{aligned} \Psi &= \left[x^2 + y^2\right]^{1/2} \quad , \quad \phi = \arctan\left(\frac{y}{x}\right) \\ x &= \Psi\cos(\phi) \quad , \quad y = \Psi\sin(\phi) \end{aligned} \tag{2.3}$$

and spherical (r, θ, ϕ) coordinates

$$\begin{aligned} r &= \left[\Psi^2 + z^2\right]^{1/2} \quad , \quad \theta = \arcsin\left(\frac{\Psi}{r}\right) \\ \Psi &= r\sin(\theta) \quad , \quad z = r\cos(\theta) \end{aligned} \tag{2.4}$$

The identity dyadic is

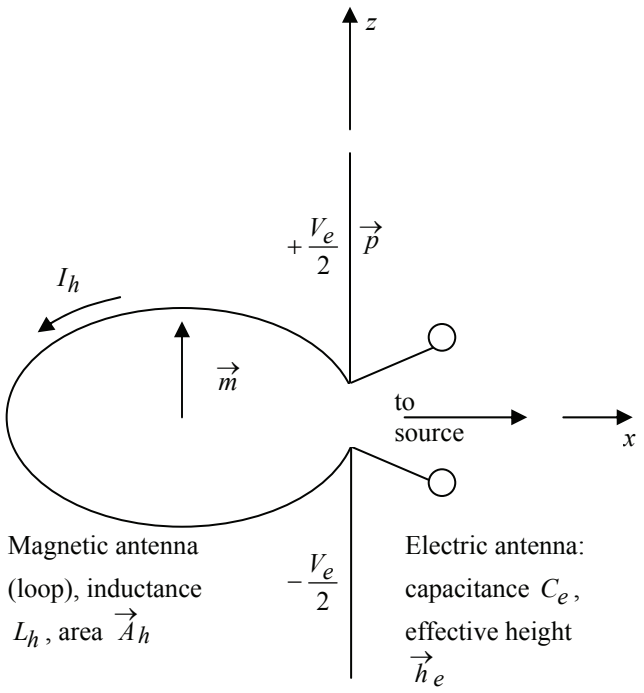

Fig. 2.1 Combined Electric and Magnetic Dipoles

$$\begin{aligned}\overleftrightarrow{1} &= \vec{1}_x\vec{1}_x + \vec{1}_y\vec{1}_y + \vec{1}_z\vec{1}_z \\ &= \vec{1}_\Psi\vec{1}_\Psi + \vec{1}_\phi\vec{1}_\phi + \vec{1}_z\vec{1}_z \\ &= \vec{1}_r\vec{1}_r + \vec{1}_\theta\vec{1}_\theta + \vec{1}_\phi\vec{1}_\phi\end{aligned} \tag{2.5}$$

and an important transverse dyadic is

$$\overleftrightarrow{1}_r = \overleftrightarrow{1} - \vec{1}_r\vec{1}_r = \vec{1}_\theta\vec{1}_\theta + \vec{1}_\phi\vec{1}_\phi \tag{2.6}$$

Dipoles have fields of the form [3]

$$\begin{aligned}\tilde{\vec{E}}_p(\vec{r},s) &= e^{-\gamma r}\left[\frac{1}{4\pi r^3}\frac{1}{\varepsilon_0}\left[3\vec{1}_r\vec{1}_r - \overleftrightarrow{1}\right]\cdot\tilde{\vec{p}}(s)\right. \\ &\quad \left. + \frac{Z_0}{4\pi r^2}s\left[3\vec{1}_r\vec{1}_r - \overleftrightarrow{1}\right]\cdot\tilde{\vec{p}}(s) - \frac{\mu_0}{4\pi r}s^2\overleftrightarrow{1}_r\cdot\tilde{\vec{p}}(s)\right] \\ \tilde{\vec{H}}_p(\vec{r},s) &= e^{-\gamma r}\left[-\frac{1}{4\pi r^2}s\vec{1}_r\times\tilde{\vec{p}}(s) - \frac{1}{4\pi r}\frac{s^2}{c}\overleftrightarrow{1}_r\times\tilde{\vec{p}}(s)\right] \\ \tilde{\vec{E}}_m(\vec{r},s) &= e^{-\gamma r}\left[\frac{\mu_0}{4\pi r^2}s\vec{1}_r\times\tilde{\vec{m}}(s) + \frac{1}{4\pi r}\frac{\mu_0}{c}s^2\overleftrightarrow{1}_r\times\tilde{\vec{m}}(s)\right] \\ \tilde{\vec{H}}_m(\vec{r},s) &= e^{-\gamma r}\left[\frac{1}{4\pi r^3}\left[3\vec{1}_r\vec{1}_r - \overleftrightarrow{1}\right]\cdot\tilde{\vec{m}}(s)\right. \\ &\quad \left. + \frac{1}{4\pi r^2}\frac{s}{c}\left[3\vec{1}_r\vec{1}_r - \overleftrightarrow{1}\right]\cdot\tilde{\vec{m}}(s) - \frac{1}{4\pi r}\frac{s^2}{c^2}\overleftrightarrow{1}_r\cdot\tilde{\vec{m}}(s)\right]\end{aligned}$$

$$c = \left[\mu_0\varepsilon_0\right]^{-1/2} \equiv \text{speed of light} \tag{2.7}$$

$$Z_0 \equiv \left[\frac{\mu_0}{\varepsilon_0}\right]^{1/2} \equiv \text{wave impedance of free space}$$

$$\gamma = \frac{s}{c} \equiv \text{propagation constant}$$

The dipole moments are related to voltage and current as

$$\begin{aligned}
\tilde{\vec{p}}(s) &= \tilde{Q}_e(s)\vec{h}_e = C_e\tilde{V}_e(s)\vec{h}_e \\
\tilde{\vec{m}}(s) &= \tilde{I}_h(s)\vec{A}_h \\
\tilde{V}_e(s) &= sL_h\,\tilde{I}_h(s) = C_eQ_e(s)
\end{aligned} \tag{2.8}$$

Previous consideration of combined electric and magnetic dipoles [3, 4, 7-11] have the dipoles at right angles and in phase to give a cardiod pattern. In this case, in the main-beam direction the ratio of the electric and magnetic fields is Z_0, including for the near-field terms. The present case is different. The dipoles are $\pi/2$ out of phase and parallel as in (2.8).

Choosing

$$\vec{h}_e = h_e\vec{1}_z \quad , \quad \vec{A}_h = A_h\vec{1}_z \tag{2.9}$$

dipoles give fields of in the form [3]

$$\begin{aligned}
\tilde{\vec{E}}(\vec{r},s) &= \tilde{\vec{E}}_p(\vec{r},s) + \tilde{\vec{E}}_m(\vec{r},s) \\
&= e^{-\gamma r}\left[\frac{1}{4\pi r^3}\frac{1}{\varepsilon_0}\left[3\vec{1}_r\vec{1}_r - \overleftrightarrow{1}\right]\bullet\vec{1}_z\,\tilde{p}(s)\right. \\
&\quad + \frac{s}{4\pi r^2}\left[Z_0\left[3\vec{1}_r\vec{1}_r - \overleftrightarrow{1}\right]\bullet\vec{1}_z\,\tilde{p}(s) + \mu_0\,\vec{1}_r\times\vec{1}_z\,\tilde{m}(s)\right] \\
&\quad \left. + \frac{s^2}{4\pi r}\left[-\mu_0\overleftrightarrow{1}_r\bullet\vec{1}_z\,p(s) + \frac{\mu_0}{c}\vec{1}_r\times\vec{1}_z\,\tilde{m}(s)\right]\right] \\
\vec{H}(\vec{r},s) &= \vec{H}_m(\vec{r},s) + \vec{H}_p(\vec{r},s) \\
&= e^{-\gamma r}\left[\frac{1}{4\pi r^3}\left[3\vec{1}_r\vec{1}_r - \overleftrightarrow{1}\right]\bullet\vec{1}_z\,\tilde{m}(s)\right. \\
&\quad + \frac{s}{4\pi r^2}\left[\frac{1}{c}\left[3\vec{1}_r\vec{1}_r - \overleftrightarrow{1}\right]\bullet\vec{1}_z\,\tilde{m}(s) - \vec{1}_r\times\vec{1}_z\,\tilde{p}(s)\right] \\
&\quad \left. + \frac{s^2}{4\pi r}\left[-\frac{1}{c^2}\overleftrightarrow{1}_r\bullet\vec{1}_z\,\tilde{m}(s) + \frac{1}{c}\vec{1}_r\times\vec{1}_z\,\tilde{p}(s)\right]\right]
\end{aligned} \tag{2.10}$$

Now, specializing to the resonant frequency $j\omega_0$, set

$$\tilde{p}(j\omega_0) = \frac{j}{c}\tilde{m}(j\omega_0) \tag{2.11}$$

which implies

$$\begin{aligned}\tilde{p}(j\omega_0) &= C_e\tilde{V}_e(j\omega_0)h_e = \frac{j}{c}\tilde{I}_h(j\omega_0)A_h \\ &= \frac{j}{c}\frac{\tilde{V}_e(j\omega_0)}{j\omega_0 \mathrm{L}_h}A_h \\ \frac{h_e}{A_h} &= \frac{1}{c}\frac{1}{\omega_0 \mathrm{L}_h \mathrm{C}_e} = \frac{\omega_0}{c}\end{aligned} \tag{2.12}$$

Note the convention here. In Fig. 2.1 $\vec{m}$ is taken as parallel to $\vec{p}$. By reversing the loop connections we could reverse the polarity of $\vec{m}$. This will interchange the roles of right- and left- handed circular polarization.

At this resonant frequency, then replace $\tilde{m}$ by $\tilde{p}$ in (2.10), and noting that

$$\begin{aligned}&\vec{1}_r \times \vec{1}_z = -\sin(\theta)\vec{1}_\phi \ , \quad \gamma_0 = \frac{j\omega_0}{c} \\ &\vec{1}_r \bullet \vec{1}_z = \cos(\theta) \ , \quad \overleftrightarrow{1}_r \bullet \vec{1}_z = -\sin(\theta)\vec{1}_\theta\end{aligned} \tag{2.13}$$

gives

$$\begin{aligned}\tilde{\vec{E}}(\vec{r}, j\omega_0) &= e^{-\gamma_0 r}\left[\frac{1}{4\pi r^3}\frac{1}{\varepsilon_0}\left[3\vec{1}_r\vec{1}_r - \overleftrightarrow{1}\right] \bullet \vec{1}_z\right. \\ &\quad + \frac{j\omega_0}{4\pi r^2}Z_0\left[3\vec{1}_r\cos(\theta) - \vec{1}_z = j\sin(\theta)\vec{1}_\phi\right] \\ &\quad \left. + \frac{\omega_0^2}{4\pi r}\mu_0\left[\vec{1}_\theta\sin(\theta) + j\sin(\theta)\vec{1}_\phi\right]\right]\tilde{p}(j\omega_0) \\ Z_0\tilde{\vec{H}}(j\omega_0) &= e^{-\gamma_0 r}\left[-\frac{1}{4\pi r^3}\frac{j}{\varepsilon_0}\left[3\vec{1}_r\vec{1}_r - \overleftrightarrow{1}\right] \bullet \vec{1}_z\right. \\ &\quad + \frac{j\omega_0}{4\pi r^2}Z_0\left[-j3\vec{1}_r\cos(\theta) + j\vec{1}_z + \sin(\theta)\vec{1}_\phi\right] \\ &\quad \left. - \frac{\omega_0^2}{4\pi r}\mu_0\left[j\sin(\theta)\vec{1}_\theta - \sin(\theta)\vec{1}_\phi\right]\right]\tilde{p}(j\omega_0)\end{aligned} \tag{2.14}$$

Now look at the farfield, the r^{-1} term, which is

$$\begin{aligned}\vec{\tilde{E}}_f(\vec{r}, j\omega_0) &= e^{-\gamma_0 r}\frac{\omega_0^2}{4\pi r}\mu_0 \sin(\theta)\left[\vec{1}_\phi + j\vec{1}_\phi\right]\tilde{p}(j\omega_0)\\ Z_0\vec{\tilde{H}}_f(\vec{r}, j\omega_0) &= e^{-\gamma_0 r}\frac{\omega_0^2}{4\pi r}\mu_0 \sin(\theta)\left[\vec{1}_\phi - j\vec{1}_\theta\right]\tilde{p}(j\omega_0)\end{aligned} \tag{2.15}$$

Here we have, noting an oscillation as $e^{j\omega_0 t}$, a far field with $\vec{\tilde{E}}_f \times \vec{\tilde{H}}_f$ in the $\vec{1}_r$ direction, and a sense of polarization given by (at a constant *r*)

$$\left[\vec{1}_\theta + j\vec{1}_\phi\right]e^{j\omega_0 t} = \left[\vec{1}_\phi + e^{j\frac{\pi}{2}}\vec{1}_\phi\right]e^{j\omega_0 t} \tag{2.16}$$

As one looks in the $\vec{1}_r$ direction this represents left-handed circular polarization (counterclockwise). By reversing the loop connections in Fig. 2.1, this would give right- handed circular polarization. Note the sin(θ) term making the pattern zero on the z axis. This antenna can then be constructed in two complementary forms which are mirror images of each other.

Note that the near-field terms (r^{-2} and r^{-3}) are not quite as simple, having radial as well as transverse components. However, these simplify on the equator ($\theta = \pi/2$).

3. Some Considerations Concerning Antenna Geometry

The previous section assumes some ideal electric- and magnetic-dipole antennas. There are various ways one might realize these. For such designs an important consideration is symmetry [24].

A first consideration is that of colocating the effective centers of the electric and magnetic dipoles. Then in Fig. 2.1 move the loop so that it is centered on the *z* axis as well as being of circular shape (approximately a body of revolution centered on the *z* axis). The electric dipole can also be a body of revolution about the *z* axis, as wall being symmetric with respect to the *xy* plane.

Consider then the geometry in Fig. 3.1. The magnetic dipole takes a form which is approximately a thin annular disk lying on the *xy* plane. As in Fig. 3.1A this interferes very little with the electric field from the electric dipole due to the symmetry with respect to the *xy* plane. The capacitance and equivalent height of the electric dipole are governed by its shape (fatness and length).

The electric dipole takes a shape which is narrow near the origin so as to have minimal interference with the magnetic field from the magnetic dipole as in Fig. 3.1B. This leads to a shape of the electric dipole much like the ACD (asymptotic conical dipole) [2, 6]. In this context one can readily calculate C_e and $\vec{h}_e$. There will be some (ideally small) interference with the magnetic field of the magnetic dipole. Detailed calculation or measurement can estimate this.

The annular-disk loop, as in Fig. 3.2, is described by

$$\begin{aligned} \Psi_1 &\equiv \text{inner radius} \\ \Psi_2 &\equiv \text{outer radius} \end{aligned} \tag{3.1}$$

There is then some effective radius, Ψ_0, for the effective area

$$\begin{aligned} A_h &= \pi\Psi_0^2 \\ \Psi_1 &< \Psi_0 < \Psi_2 \end{aligned} \tag{3.2}$$

For highly inductive loops with

$$\Psi_2 - \Psi_1 << \Psi_0 \tag{3.3}$$

then, approximately, we have

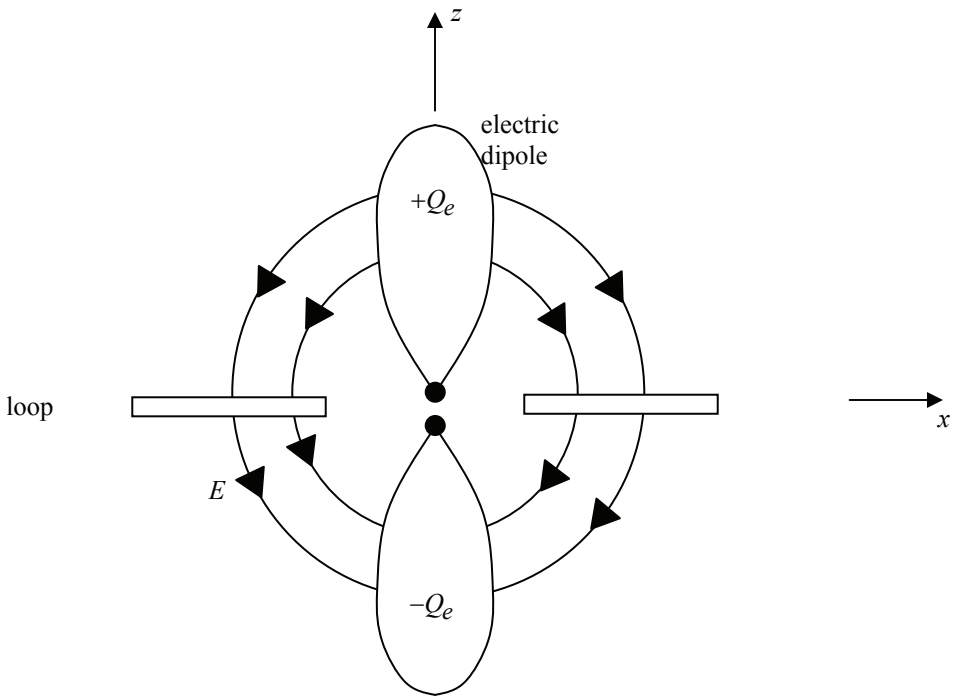

A. Electric-field distribution from electric dipole.

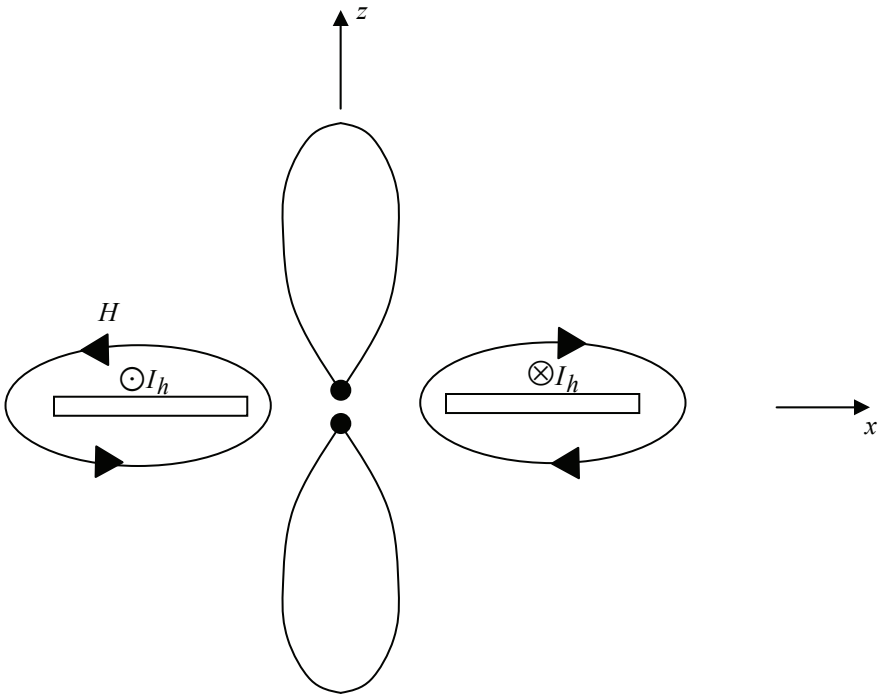

B. Magnetic-field distribution from magnetic dipole.

Fig. 3.1 Symmetric Combination of Electric and Magnetic Dipoles

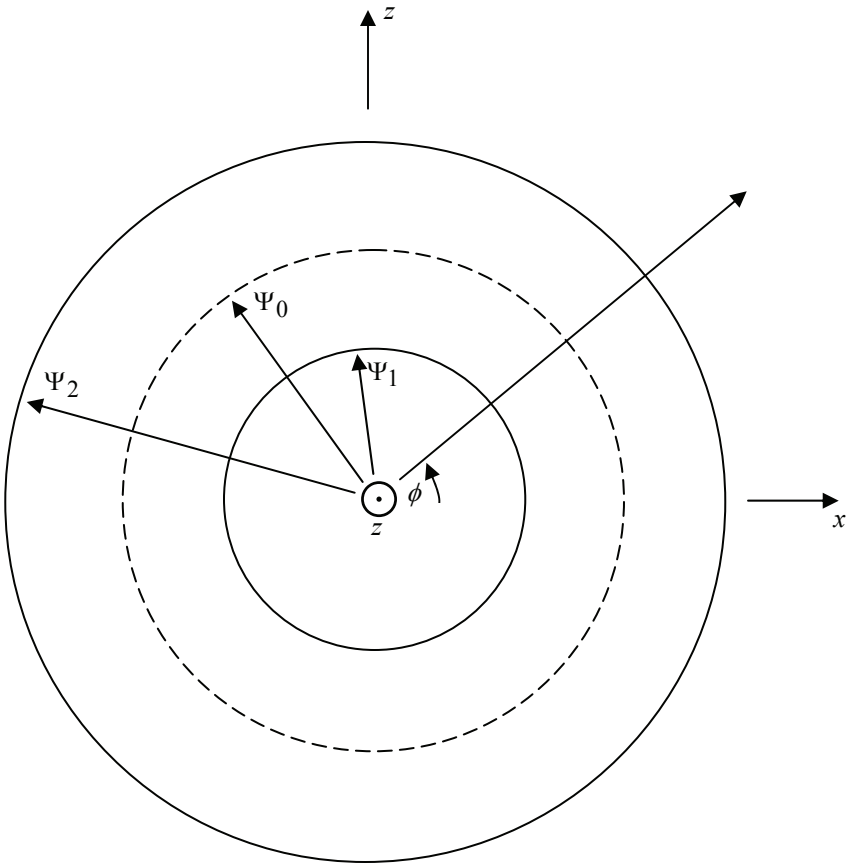

Fig. 3.2 Annular-Disk Loop

$$\Psi_0 \simeq \frac{1}{2}[\Psi_1 + \Psi_2] \tag{3.4}$$

For low-inductance loops without the (3.3) approximation one can resort to a more detailed calculation.

For such highly inductive loops we can approximate the loop by a thin toroidal loop as in Fig. 3.3. In this case we can use the equivalent radius, b, of a strip as [22]

$$b = \frac{1}{4}[\Psi_2 - \Psi_1] \tag{3.5}$$

We then go to the well-known inductance formula [23]

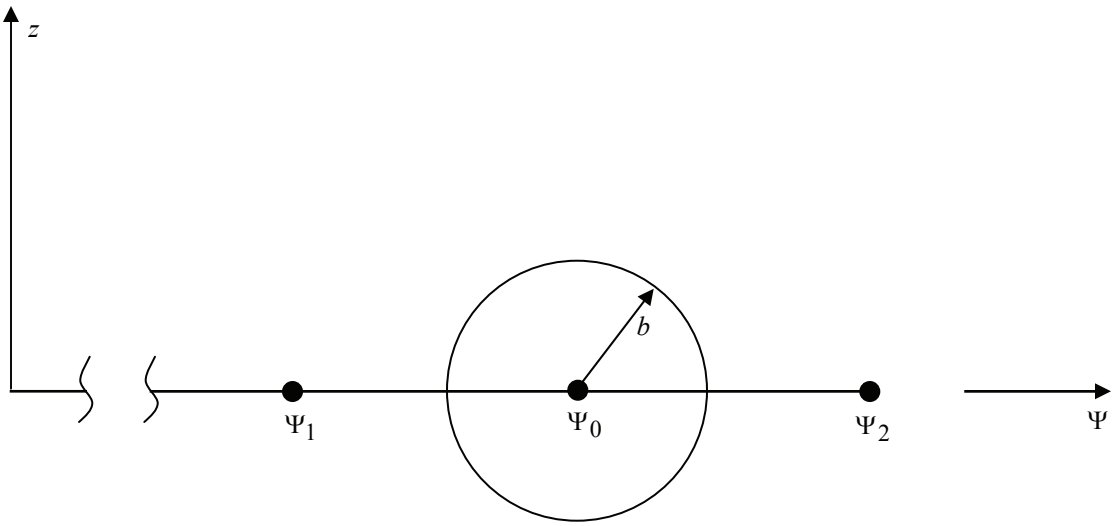

Fig. 3.3 Equivalent Toroidal Loop

$$\begin{aligned} \mathrm{L}_h &\simeq \mu_0 \Psi_0 \left[\ell n\left(\frac{8\Psi_0}{b} \right) - 2 \right] \\ &\simeq \mu_0 \Psi_0 \left[\ell n\left(\frac{32\Psi_0}{\Psi_2 - \Psi_1} \right) - 2 \right] \end{aligned} \tag{3.6}$$

The annular disk will have some (ideally small) thickness. However, at the edges one may wish to thicken them to minimize losses [19] and high electric fields. Consider a rollup on these edges as in Fig. 3.4. As shown in [5] a rollup of radius *b'* is approximately equivalent to a disk edge extending out an extra distance of *b'* to the ideal-disk outer radius of Ψ_2. The same result can be applied to a rollup on the inner edge, extending Ψ_1 to a radius smaller by the *b'* of the inner rollup.

Another consideration for loop design concerns higher-order terms in the current and charge on the loop. If the loop is cut at one place to connect the source, there is also a charge displacement across the loop, particularly at high frequencies. This can be avoided by a technique used in the MGL (multigap loop) [1]. As illustrated in Fig. 3.5 one can suppress the electric-dipole term by cutting the loop into two half-loops driven in parallel. This reduces the loop parameters as

$$\begin{aligned} A_h &= \frac{1}{2} A_{h_1} = \frac{1}{2} \pi \Psi_0^2 \\ \mathrm{L}_h &= \frac{1}{4} \mathrm{L}_{h_1} \simeq \frac{1}{4} \Psi_0 \left[\ell n\left(\frac{8\Psi_0}{b} \right) - 2 \right] \end{aligned} \tag{3.7}$$

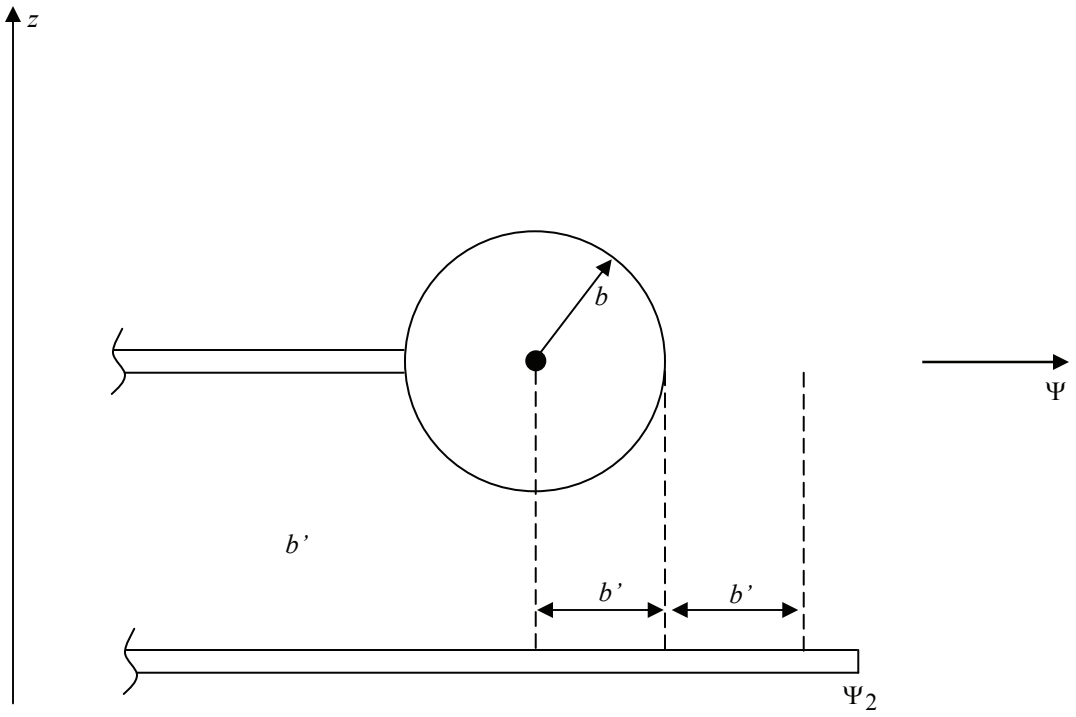

Fig. 3.4. Rollup to Avoid Sharp Edge of Annular Disk: Illustrated for Outer Edge.

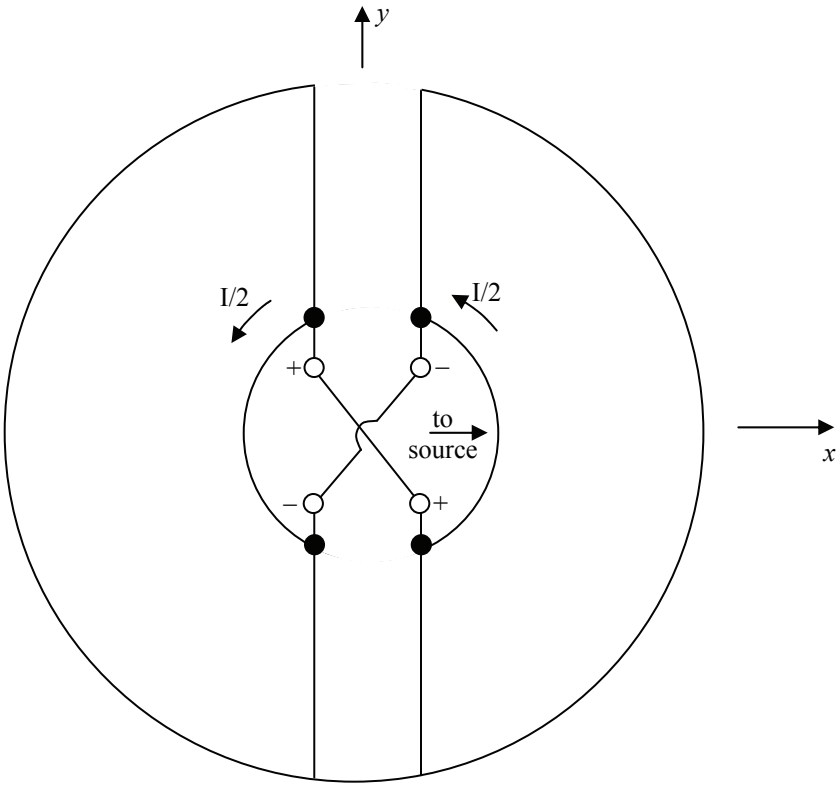

Figure 3.5 Loop Connections to Remove Electric-Dipole Term

where the subscript "1" indicates the parameter for the single-turn loop, being now applied to the half-turn loop. Here L_h needs to be increased some to allow for the lead inductances. This needs to be taken into account when balancing the electric- and magnetic-dipole moments.

In balancing the electric- and magnetic-dipole moments there are then some steps to follow:

1. Adjust C_e and L_h to match desired ω_0.
2. Adjust $\vec{h}_e$ and $\vec{A}_h$ to match $|\vec{p}|$ to $|\vec{m}|/c$.

This gives two constraints on four parameters. Noting the scaling, if one chooses one of the parameters, this still leaves three, giving various possibilities. For the electric dipole $\vec{h}_e$ and C_e are independent within geometric constraints. Similarly, for the magnetic dipole $\vec{A}_h$ and L_h are independent within geometric constraints. One of these constraints on how much the parameters can be varied is the electrically small constraint. Note that we can add to C_e and L_h, if needed by "trimming" elements which do not contribute to $\vec{h}_e$ and $\vec{A}_h$, respectively.

4. Combination of Antenna with Switched Oscillator

Having chosen our antenna parameters, we can now consider matching the antenna to a source. Let us consider the switched oscillator as such a source [20] as indicated in Fig. 4.1. The oscillator is approximated as a quarter-wave resonant transmission line. While the center conductor is charged, the blocking capacitor C_b keeps the charging voltage V_0 off the antenna. The closing switch is represented by a voltage which we can approximate as V_0/s, except for the (sufficiently fast) risetime.

With a transmission-line characteristic impedance of Z_c, the switched oscillator has a source impedance due to a short circuit at the switch end of

$$\tilde{Z}_s(s) = Z_c \frac{1-e^{-2\gamma\ell}}{1+e^{-2\gamma\ell}} = Z_c \tanh(\gamma\ell) \tag{4.1}$$

The open-circuit voltage out of the switched oscillator is

$$\tilde{V}_{oc}(s) = \frac{V_o}{s}\frac{2e^{-\gamma\ell}}{1+e^{-2\gamma\ell}} = \frac{V_o}{s}\cosh^{-1}(\gamma\ell)$$

$$\gamma = \frac{s}{\mathrm{v}} = \text{propagation constant}$$

v = propagation speed in switched oscillator

$s \equiv \Omega + j\omega \equiv$ Laplace-transform variable or complex frequency (4.2)

$\sim \equiv$ two-sided Laplace transform

Like the antenna, the switched oscillator is tuned to ω_0, for which (near ω_0)

$$\omega = \omega_0 + \Delta\omega$$

$$\gamma\ell = jk\ell = j\frac{\ell}{\mathrm{v}}\left[\omega_0 + \Delta\omega\right]$$

$$\frac{\ell\omega_0}{\mathrm{v}} = \frac{\pi}{2}$$

$$\gamma\ell = j\frac{\pi}{2}\left[1+\frac{\Delta\omega}{\omega_0}\right]$$

$$\tilde{V}_{oc}(j\omega) = \frac{V_o}{j\omega}\cos^{-1}\left(\left[\omega_0+\Delta\omega\right]\frac{\ell}{\mathrm{v}}\right) = \frac{V_o}{j\omega}\cos^{-1}\left(\frac{\pi}{2}\left[1+\frac{\Delta\omega}{\omega_0}\right]\right)$$

$$= -\frac{V_o}{j\omega}\sin^{-1}\left(\frac{\pi}{2}\frac{\Delta\omega}{\omega_0}\right) \simeq \frac{-V_o}{j\omega}\frac{2}{\pi}\frac{\omega_0}{\Delta\omega}$$

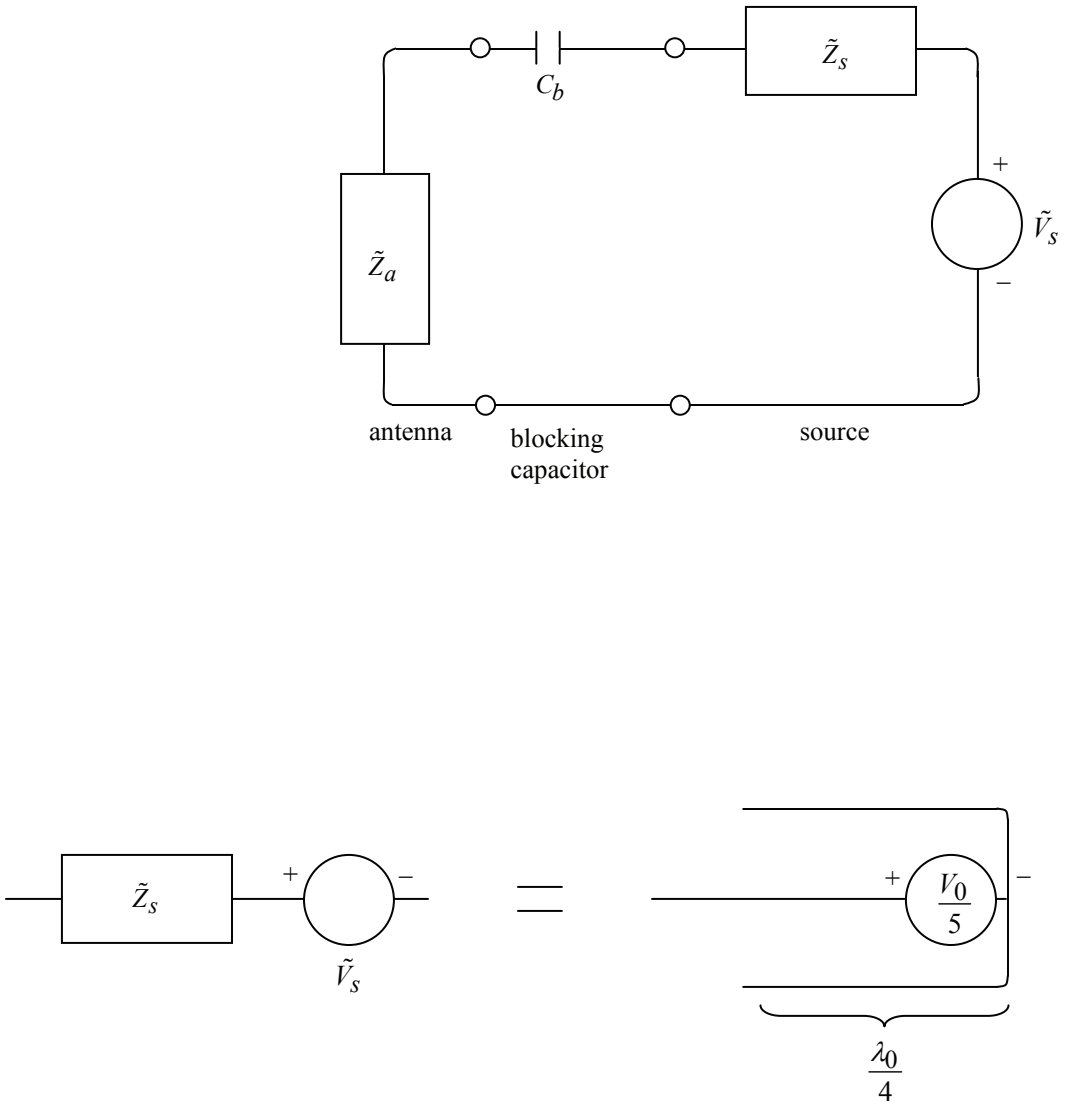

Fig. 4.1 Switched Oscillator Driving Antenna

$$
\begin{aligned}
&\simeq jV_0\frac{2}{\pi}\frac{1}{\Delta\omega}\\
\tilde{Z}_s(j\omega) &= Z_c j\tan\left(\left[\omega_0+\Delta\omega\right]\frac{\ell}{\mathrm{v}}\right) \simeq Z_c j\cos^{-1}\left(\frac{\pi}{2}\left[1+\frac{\Delta\omega}{\omega_0}\right]\right)\\
&\simeq -Z_c j\sin^{-1}\left(\frac{\pi}{2}\frac{\Delta\omega}{\omega_0}\right) \simeq -Z_c j\frac{2}{\pi}\frac{\omega_0}{\Delta\omega}
\end{aligned}
\tag{4.3}
$$

The antenna has an impedance

$$
Z_a(s) = \left[\frac{1}{s\mathrm{L}_a} + s\mathrm{C}_a\right]^{-1} = sL_a\left[1 + s^2\mathrm{L}_a\mathrm{C}_a\right]^{-1} = sL_a\left[1+s^2\omega_0^{-2}\right]^{-1} \tag{4.4}
$$

Near ω_0 this is

$$
Z_a(j\omega) = j\omega\mathrm{L}_a\left[1-\left[\frac{\omega}{\omega_0}\right]^2\right]^{-1} \simeq j\omega_0 L_a\left[\frac{-2\Delta\omega}{\omega_0}\right]^{-1} = \frac{-j\omega_0^2 L_a}{2\Delta\omega} \tag{4.5}
$$

This allows us to set (near ω_0)

$$
\begin{aligned}
Z_{tot}(j\omega) &= Z_a(j\omega) + Z_s(j\omega) \simeq -j\left[\frac{\omega_0\mathrm{L}_a}{2} + Z_c\frac{2}{\pi}\right]\frac{\omega_0}{\Delta\omega}\\
f_a &+ f_0 = 1\\
f_a &= \frac{\omega_0\mathrm{L}_0}{2}\left[\frac{\omega_0\mathrm{L}_a}{2} + Z_c\frac{2}{\pi}\right]^{-1} = \left[1 + \frac{Z_c}{\omega_0\mathrm{L}_a}\frac{4}{\pi}\right]^{-1}\\
f_0 &= Z_c\frac{2}{\pi}\left[\frac{\omega_0\mathrm{L}_a}{2} + Z_c\frac{2}{\pi}\right]^{-1} = \left[1 + \frac{\omega_0\mathrm{L}_a}{Z_c}\frac{\pi}{4}\right]^{-1}\\
Z_a(j\omega) &= f_a Z_{tot}(j\omega)\\
Z_c(j\omega) &= f_0 Z_{tot}(j\omega)
\end{aligned}
\tag{4.6}
$$

The combination of the source with the antenna can be considered as a voltage divider. As f_a increases the fraction of source voltage on the antenna increases. This implies for a given ω_0, a large L_a and associated small C_a. However, there are other considerations, including large $\vec{p}$ and $\vec{m}$. Note that the impedance of C_b, being finite at ω_0, is neglected for this analysis.

With the switched oscillator matched to the antenna, we next need to estimate the dipole moments at resonance. The antenna voltage near resonance is

$$\tilde{V}_a(j\omega) = f_a \tilde{V}_{oc}(j\omega) \simeq j f_a \; V_o \; \frac{2}{\pi}\frac{1}{\Delta\omega} \to \infty \text{ as } \omega \to \omega_0 \tag{4.7}$$

Of course, this is not exact, since we have neglected losses which move the resonance, at least a little, into the left-half s plane.

Now reinterpret (4.7) in terms of s to achieve a dominant term near resonances as

$$\begin{aligned} \tilde{V}_a(s) &\simeq -f_0 V_0 \frac{2}{\pi}\frac{1}{s - s_0} \\ s_0 &= j\omega_0 \\ s &= j\omega = j\left[\omega_0 + \Delta\omega\right] \end{aligned} \tag{4.8}$$

Including the conjugate pole we have

$$\begin{aligned} \tilde{V}_a(s) &\simeq -f_a V_0 \frac{2}{\pi}\left[\left[s - s_0\right]^{-1} + \left[s - s_0^*\right]^{-1}\right] \\ s_0^* &= -j\omega_0 \end{aligned} \tag{4.9}$$

In time domain this resonant term is

$$\begin{aligned} V_a(t) &\simeq -f_a V_0 \frac{2}{\pi}\left[e^{s_0 t} + e^{s_0^* t}\right] u(t) \\ &= -f_a V_0 \frac{4}{\pi}\cos(\omega_0 t) u(t) \end{aligned} \tag{4.10}$$

This gives, for small losses, the time-domain form of the resonance at modestly early times. There are other transients not included here. Note also that there is a delay due to the length of the switched oscillator which is not included in (4.10). Subtracting this delay gives

$$V_a(t) = f_a V_0 \frac{4}{\pi}\sin\left(\omega_0 t - \frac{\pi}{2}\right) u\left(t - \frac{\pi}{2\omega_0}\right) \tag{4.11}$$

which needs to be multiplied by $e^{-\alpha\left[t - \frac{\pi}{2\omega_0}\right]}$ to account for radiation and other losses.

From Section 2 we have

$$\tilde{p}(s) = C_e \tilde{V}_a(s) = C_e f_a \tilde{V}_{oc}(j\omega) \tag{4.12}$$

from which the time-domain form is

$$\tilde{p}(t) = C_e V_a(t) \tag{4.13}$$

It is this that we wish to maximize, noting that $m(t)$ is constrained to this with a $\pi/2$ phase shift. Going back to (2.14) gives the far fields.

5. Concluding Remarks

In this new form of mesoband radiator the energy sloshes back and forth between inductance and capacitance (in both the source and antenna), instead of being lost in a resistive termination. Of course there are still the radiation losses and losses in the conductors, dielectrics, and the high-voltage switch. These losses may also affect the quadrature relation between $\tilde{p}$ and $\tilde{m}$, giving some (small) dependence on ϕ. The foregoing is, after all, a high-Q approximation.

While our primary concern is with the far fields, there are corrections for the near fields depending on the distance to the target. There are also higher-order antenna terms (quadrupole, etc.)

References

1. C. E. Baum, "The Multi-Gap Cylindrical Loop in Non-Conducting Media", Sensor and Simulation Note 41, May 1967.
2. C. E. Baum, "An Equivalent-Charge Method for Defining Geometries of Dipole Antennas", Sensor and Simulation Note 72, January 1969.
3. C. E. Baum, "Some Characteristics of Electric and Magnetic Dipole Antennas for Radiating Transient Pulses", Sensor and Simulation Note 125, January 1971.
4. J. S. Yu, C.-L. J. Chen, and C. E. Baum, "Multipole Radiations: Formulation and Evaluation for Small EMP Simulators", Sensor and Simulation Note 243, July 1978.
5. D. V. Giri and C. E. Baum, "Equivalent Displacement for a High-Voltage Rollup on the Edge of a Conducting Sheet", Sensor and Simulation Note 294, October 1986.
6. G. D. Sower, "Optimization of the Asymptotic Conical Dipole", Sensor and Simulation Note 295, October 1986.
7. E. G. Farr and J. S. Hofstra, "An Incident Field Sensor for EMP Measurements", Sensor and Simulation Note 319, November 1989.
8. C. E. Baum, "General Properties of Antennas", Sensor and Simulation Note 330, July 1991; IEEE Trans. EMC, 2002, pp. 18-24.
9. F. M. Tesche, "The p x m Antenna and Applications to Radiated Field Testing of Electrical Systems Part 1—Theory and Numerical Simulations", Sensor and Simulation Note 407, July 1997.
10. F. M. Tesche and T. Karlsson, "The p x m Antenna and Application to Radiated Field Testing of Electrical Systems Part 2—Experimental Considerations", Sensor and Simulation Note 409, August 1997.
11. E. G. Farr, C. E. Baum, W. D. Prather, and T. Tran, "A Two-Channel Balanced-Dipole Antenna (BDA) With Reversible Antenna Pattern Operating at 50 Ohms", Sensor and Simulation Note 441, December 1999.
12. C. E. Baum, "Antennas for the Switched-Oscillator Source", Sensor and Simulation Note 455, March 2001.
13. C. E. Baum, "Differential Switched Oscillators and Associated Antennas", Sensor and Simulation Note 457, June 2001.
14. C. E. Baum, "Compact, Low-Impedance Magnetic Antennas", Sensor and Simulation Note 470, December 2002; Proc. ICEAA 2005, Turin, Italy, pp. 7-10.
15. C. E. Baum, "Differential Switched Oscillators and Associated Antennas, Part 2", Sensor and Simulation Note 484, November 2003.
16. C. E. Baum, "More Antennas for the Switched Oscillator", Sensor and Simulation Note 493, August 2004.
17. C. E. Baum, "Compact Electric Antennas", Sensor and Simulation Note 500, August 2005.
18. E. G. Farr, L. H. Bowen, C. E. Baum, and W. D. Prather, "The Folded Horn Antenna", Sensor and Simulation Note 520, December 2006.
19. J. S. Tyo and C. E. Baum, "Reduced Skin Loss at the Edges of a Conducting Plane Using High-Voltage Rollups", Measurement Note 51, April 1997.
20. C. E. Baum, "Switched Oscillators", Circuit and Electromagnetic System Design Note 45, September 2000.
21. W. D. Prather, C. E. Baum, F. J. Torres, F. Sabath, and D. Nitsch, "Survey of Worldwide High-Power Wideband Capabilities", IEEE Trans. EMC, 2004, pp. 335-344.
22. R. W. P. King, *The Theory of Linear Antennas*, Harvard U. Press, 1956.
23. W. R. Smythe, *Static and Dynamic Electricity, 3rd ed.*, McGraw Hill, 1968.
24. C. E. Baum and H. N. Kritikos (eds.), *Electromagnetic Symmetry*, Taylor & Francis, 1995.